Progress in Additive Manufacturing
https://doi.org/10.1007/s40964-025-01426-5

RESEARCH

3D-printing of embedded resistive flex sensor, process development, and application to the custom rhythm game

Giulia Gaudenzi[1] · **Miriam Seiti**[1] · **Antonio Fiorentino**[1]

Received: 16 June 2025 / Accepted: 6 November 2025
© The Author(s) 2025

Abstract

Sensors are devices that can respond to an input with a measurable output, providing information about variations in the input source. Additive Manufacturing (AM) plays a pivotal role in the fabrication on novel sensors, offering new opportunities for sensor design and performance optimization using a wide range of materials at a relatively low cost. While the fabrication by the material extrusion technique (MEX) of commercial materials has been investigated in the literature, including the use of conductive PLA filament for strain gauge sensors, the systematic understanding of how printing parameters should be optimized based on the material and its intended function is still limited. Moreover, an analysis of how this printing process and the design affect the final printing, hence sensor performance outcomes, is still lacking. These aspects take on greater importance when a process is used in a less common context, as in the case of sensor printing. In this work, a robust and repeatable MEX process for the fabrication of PLAc strain gauge-based embedded sensors is proposed. Protopasta™ conductive PLA (PLAc) was adopted to print the sensor within an insulating PLA material (PLA). Key process parameters, including pre-printing idle time, ironing, and the number of sensors printed on the same substrate, were thoroughly evaluated. Then, strain gauge-based samples were fabricated under different printing conditions (idle pre-printing time for PLAc, optimal printing values, optimal design) to investigate and assess the robustness of the process. The evaluation was carried out by measuring, comparing, and analysing the relationship between the cross-section and electrical resistance of the samples. The optimal conditions that enhance the repeatability of the process were identified. Furthermore, the strain gauge-based sensors were characterised under bending conditions and showed a linear behaviour of the electrical resistance with the increasing curvature radius. Finally, the developed sensors were implemented in a rhythm game demonstrator, validating their practical functionality. Overall, the research provides a robust methodology to optimize the printing of a flexible sensor, leveraging the advantages of AM to produce reliable, ready-to-use devices.

keyword MEX · Process optimisation · Printed electronics · Strain gauges · Embedded sensors · Flexible sensors

1 Introduction

Additive Manufacturing (AM) includes a wide variety of technologies that, by adding material, lead to a complete part. A variety of approaches and materials can therefore be selected to fabricate parts for industrial [1, 2] and biomedical [3–7] fields, for sensing purposes [8, 9], in soft robotics, and also to make hydrogels [10–12].

The material extrusion (MEX) process is one of the most used AM technologies [13–15]. Its large usage is mostly related to the ease of use, the freedom in the design, the low costs of both machinery and material, and the wide variety of applications, from sensing components to rapid tooling [16–18].

In the last decade, researchers have investigated the possibility of producing functional sensors using AM [4, 10, 19–21]. This characteristic is engaging when fabricating the so-called embedded sensors, where a different material surrounds the conductive one and it is used as an encapsulator [22–24]. Amongst the materials that can be printed

✉ Giulia Gaudenzi
giulia.gaudenzi@unibs.it

Miriam Seiti
miriam.seiti@unibs.it

Antonio Fiorentino
antonio.fiorentino@unibs.it

[1] Department of Mechanical and Industrial Engineering, University of Brescia, Brescia, Italy

Published online: 03 December 2025

by MEX, the polymeric ones are particularly appreciated because of their low cost and the possibility of enriching their properties with additives. For instance, carbon is commonly used as additive [15, 25–27] due to its conductive properties that can be correlated to an increase in electrical conductivity and mechanical stress [16, 28, 29]. In literature, two conductive commercial materials have mainly been investigated: Cu and carbon-loaded PLA (Electrifi™ and Protopasta™) [30–33]. The Cu-based one has better conductive properties but produces heavy wear on the nozzle. Hence, hard and wear-resistant nozzles are required for printing. Carbon-loaded PLA (PLAc) exhibits significantly lower wear of the nozzle. Research has been conducted on its potential applications, primarily focusing on its use as a strain gauge material [34], but the understanding of how printing parameters should be optimized based on the material and its intended function is still limited. Also an analysis of how the process and the design can affect the final print quality is still lacking. These aspects are crucial when the MEX process is used for printed electronics, characterized by miniaturized microscale dimensions and low printing times, with respect to massive parts. In particular, when low print times are involved, the initial printing transient or the process fluctuations can be predominant and significantly alter the part properties. As a consequence, printed parts may be highly variable in the final performance. This aspect is less significant for large parts, where local differences are spread around a larger volume, and the properties of the final part are averagely more uniform and constant amongst the part itself and its replicates. For these reasons, the present research primarily focuses on the development of a robust and repeatable MEX process for the fabrication of PLAc 3D printed sensors. In particular, the research initially studies the process feasibility leading to an improvement of the printing parameters with respect to those reported in the technical datasheet of the PLAc material [35]. Process reliability and repeatability was further analysed. As a result, a printing protocol that stabilise the process was developed to reduce the variability amongst the printed sensors. Moreover, sensors were printed according to the protocol, and their behaviour was characterized. Finally, the developed process was adopted to fabricate a proof-of-concept demonstrator.

The experimental methodology is divided into three main steps (Table 1). First, the effects of the main process parameters on the MEX of PLAc are investigated to identify their optimal values. Preliminary printing tests allow to evaluate the effects of the printing procedure on the sensor

Table 1 Summary of the research approach

Step	Focus	Goal	Method	Result
Process characterization	Main Process Parameters	Identifying the optimal values for temperature (T) and layer height (h) to print PLAc	Printing of benchmarks for selected ranges of parameters	The best printing parameters set is: T = 220 °C h = 0.15 mm Other: w_0 = 0.45 mm v = 25 mm/s Flow 100%
	Preliminary printing tests of the sensor (strain gauge)	Evaluating the effects of the printing procedure (printing transient, printing order, and ironing) on the sensor properties	Printing of sensors under different conditions. Measurement of the sample cross-section and electrical resistance	Initial transient and print order influence the cross-section of the sensor (A) and its resistance (R). Ironing reduces the repeatability of the process
	Experimental campaign	The optimum procedure for assessing the manufacturing approach, experimental campaign	Deepen the investigation into the relevance of pre-printing time (30 s, 90 s, 180 s, and 330 s) on R_0-12 sensor design	The 180 s is the pre-printing time that showed lower variance
Sensor characterisation	Sensor flex response	Investigating the device behaviour under bending forces and validating the sensor	Bending test. N = 1 and N = 3 bent around cylinders of 120 mm and 60 mm radii	A linear correlation between the bending and the resistance values was demonstrated. Uniform Gauge Factor (14 ± 2.3)
Case study	Sensor adoption	Demonstrate the exploitability of the process and sensor developed	Fabrication of sensors for a rhythm game	Working device

properties and to determine the optimal printing protocol towards a more repeatable process. The second step focuses on the printed sensors characterisation and validation under flex deformation. Sensors were tested under bending conditions with constant curvature, showing a linear behaviour of the electrical resistance with the increasing curvature radius, and their gauge factor was further calculated. The third step illustrates the exploitation of the sensor developed in a real device. The case study adopted consists of a rhythm game with 3D-printed strain gauges. In such games, the player must replicate a specific sequence of sounds or colours by pressing some keys on a device. Even though they are mostly known for recreational purposes, they are also useful for educative, sport, and medical reasons. The literature shows that such devices can enhance performance and motivation in skiers [36], improve the reading abilities of children [37], support focus and motivation in children with disabilities through the teaching of manual signs [38], and develop psychosocial skills in individuals with ADHD through playful methods [39]. Therefore, custom device development can be of relevant use in personalised therapy.

Overall, the research demonstrates the capability of the developed MEX process protocol to fabricate resistive sensors which are suitable for standard applications but also custom devices.

2 Process characterisation

The goal of the process characterisation step is to identify the proper process parameters to print a sensor. Accordingly, the main process parameters, temperature (T) and layer height (h) for printing PLAc on the PLA substrate were identified by printing three benchmarks (Figs. 1, 2), as summed in Table 2. The focus was then set on strain gauge manufacturing. In particular, the strain gauge consists of a short line (Fig. 3), which requires a few seconds to be printed. Within this time, the initial settling of temperature or extruding pressure can prevent the achievement of a steady-state deposition of material. Therefore, the pre-printing conditions (time for pre-printing a previous third item, for material resting in the nozzle at high temperature) were investigated to evaluate their effects on the cross-section (width, thickness, and area) and electrical resistance of the sensor. Furthermore, the strong relationship between the resistance at rest (R_0) and the area (A) suggests that it is possible to evaluate the sensor behaviour by measuring the electrical resistance [40]. Overall, data showed that pre-printing conditions, mainly the pre-printing time, represent an initial process transient. This affects the quality and repeatability of the printed sensors. Accordingly, an experimental campaign was conducted to outline the optimal initial pre-printing time that guaranteed the most stable process (minimum variance amongst the printed sensors).

Experimental tests were conducted using an Ultimaker™ 3 extended printer with Cura™ slicing software. The commercial filaments Protopasta™ Conductive PLA (PLAc) and Ultimaker™ PLA pearl white (PLA) were selected to print the sensor and the substrate, respectively. Nozzle AA 0.4 was used for both materials. PLA filament was printed using the default profile of PLA. The printing process of PLAc was investigated at different levels according to the process characterization step of the workflow (Table 1).

2.1 Process parameters identification

The choice of printing parameters is fundamental for good shape and desirable mechanical and electrical properties. To select the optimal values, three benchmarks (chosen amongst the most spread ones on the web) were adopted to test the effects of layer height (h) and temperature (T) parameters. The test and the best results obtained are shown in Table 2. In particular, three h values (0.05, 0.10, and 0.15 mm) were tested at different T (ranging from 195 to 230 °C with

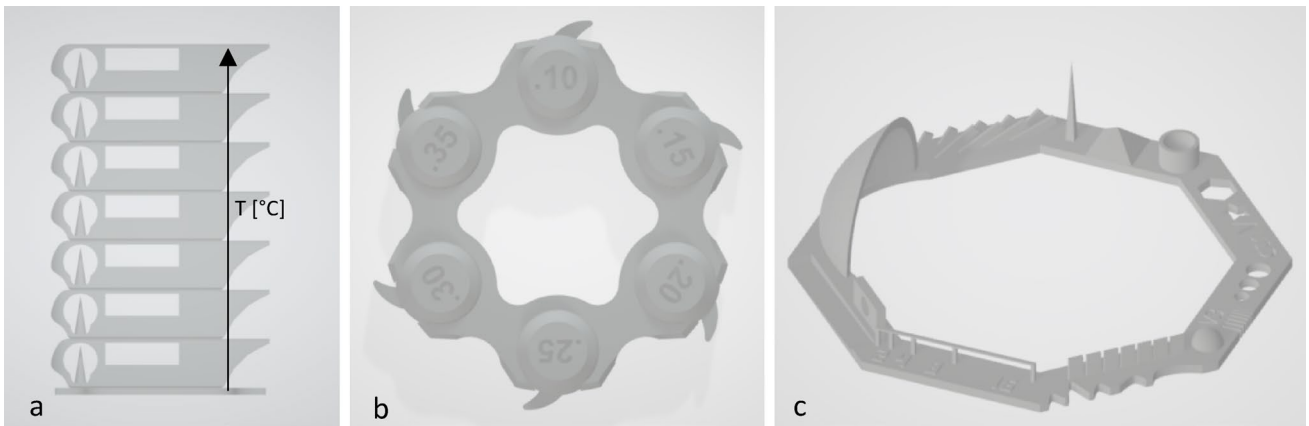

Fig. 1 Benchmarks CAD. Temperature tower (**a**), octagon (**b**), clearance tolerance test (**c**)

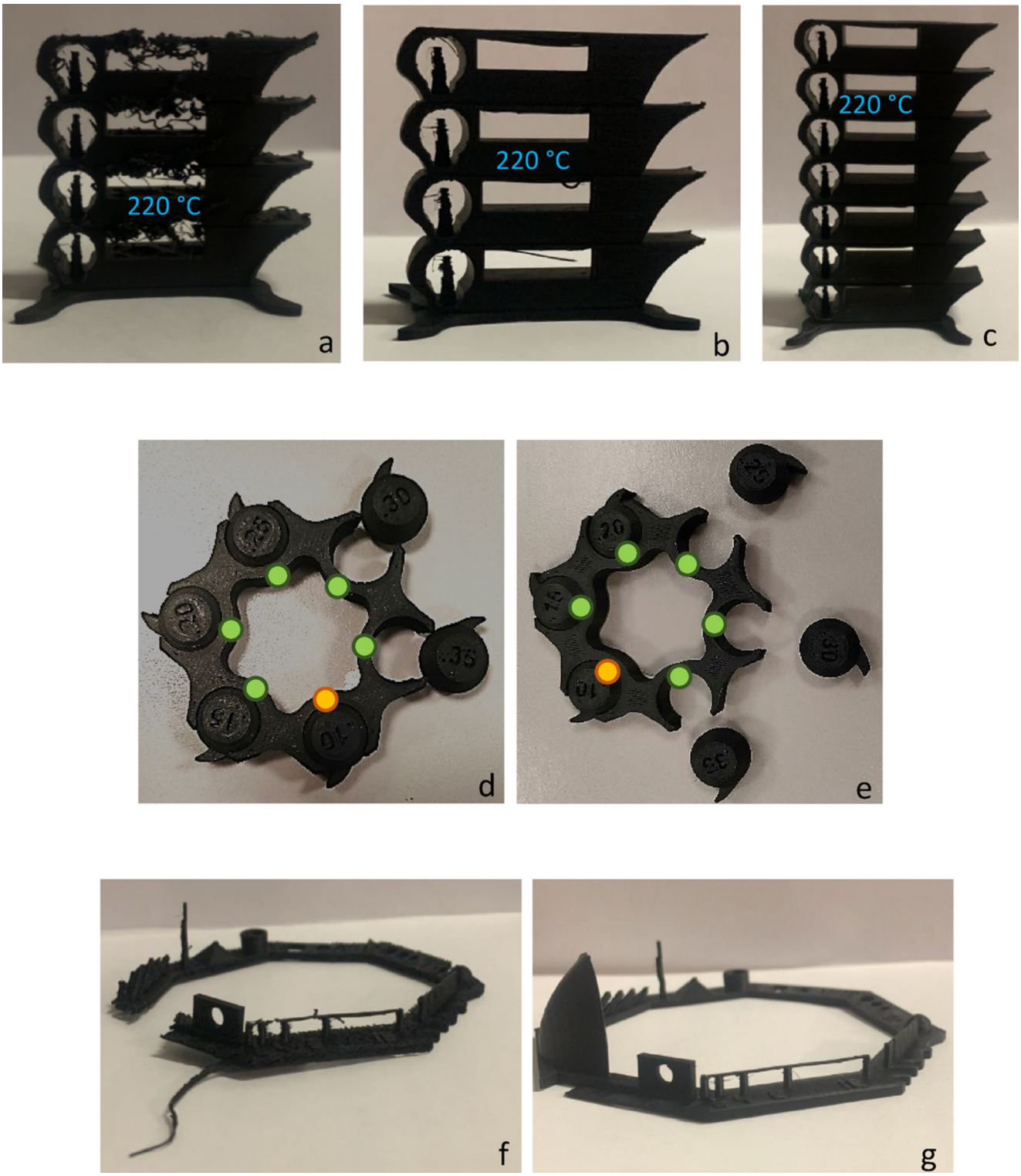

Fig. 2 Temperature towers for the layer heights: **a** h = 0.05 mm with temperature ranging from 215 to 230 °C, **b** h = 0.10 mm with temperature ranging from 210 to 225 °C, and **c** h = 0.15 mm with temperature ranging from 215 to 225 °C. Clearance tolerance test at T = 220 °C for **d** h = 0.10 mm and **e** h = 0.15 mm, and without the welding bead. Octagon benchmark at T = 220 °C for **e** h = 0.10 mm and **f** h = 0.15 mm

Table 2 Experimental test: Tested range of process parameters and optimal temperature (T) and layer height (h) for the Protopasta™ Conductive PLA (PLAc) filament

Tested parameters	Range	Optimum value	Units
Layer height (h)	0.05–0.10–0.15	0.15	[mm]
Temperature (T)	195÷230	220	[°C]
Printing speed (v)	25		[mm/s]
Flow rate	100%		
Line width	0.45		[mm]
Nozzle	Print Core AA 0.4		

increments of 5 °C). The maximum temperature value was limited by material degradation and nozzle clogging. Other process parameters were kept constant, and a printing speed of 25 mm/s was used. The plate was heated at a temperature of 60 °C, and a 100% flow rate was adopted, as suggested by the producer [41]. In addition, since the present flex sensor is a few layers thick, the material printing profile was edited to keep all printing parameters from the first layer.

Common benchmark geometries were used to evaluate the outcomes of the process parameters: temperature tower, clearance tolerance test, and octagon (Fig. 1). The temperature tower allows us to determine the feasibility of long bridges and spikes as the temperature varies. The clearance tolerance test can be used to evaluate the geometrical precision of the printing process; it consists of the printing of an all-in-one spherical coupling using different clearance values. Finally, the octagon design tests the feasibility of small features such as thin bridges, grooves, convex and concave surfaces, overhangs, warping, and spikes.

The evaluation of the results was carried out by considering the presence of printing defects. The temperature tower excluded the h=0.05 mm layer height from further investigations since printing was not continuous (Fig. 2a). Considering the remaining layer heights (Fig. 2b, c), printing results are promising in the temperature range of 215÷225 °C. A temperature of 220 °C provides a slight improvement of the printed details, even though local defects, such as spikes, misalignment, or stringing, are present, but anyway less. Accordingly, the following benchmarks were fabricated at 220 °C. The clearance tolerance test was performed using h=0.10 mm (Fig. 2d) and 0.15 mm (Fig. 2e). The starting points of the layer depositions were randomized to avoid the formation of a thick welding bead, which would interfere with the movement of the spheres. Results show that the relative movement of the spheres is possible from a clearance of 0.10 mm for both layer heights, while that octagon tests show warping and low accuracy, associated with nozzle clogging for thin features (Fig. 2f). This can be solved by adopting a layer height of h=0.15 mm (Fig. 2g).

Considering adhesion on the substrate, continuity of the line, and qualitative replication of the CAD design, the benchmark tests outlined the best parameter values of h=0.15 mm and T=220 °C when printing with v=25 mm/s, 100% flow rate, and 0.45 mm line width.

2.2 Printing sensor preliminary test

The flex sensor consists of a relatively small PLAc strain gauge (Fig. 3), printed on a PLA substrate. The sensor and substrate are 0.15 mm and 0.45 mm thick, respectively (corresponding to 1 and 3 layers, according to Table 2) for a total of 0.6 mm. By using the dual-material extrusion process, the small sensor can be printed in less than 10 s. As a

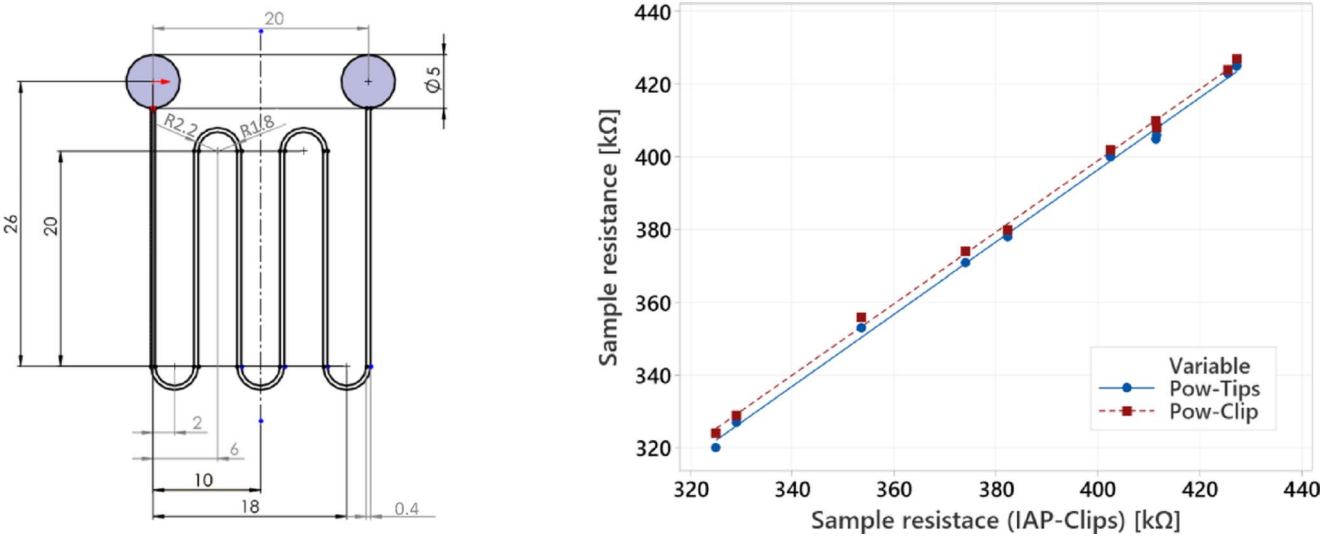

Fig. 3 Geometry of the sensor (a strain gauge, one layer thick, upon a three-layer substrate) with dimensions in mm. Comparison of the resistances at rest measured using probes with a powermeter, clips, and an impedance analyser, and clips connected to a powermeter, the measurements were taken for ten samples

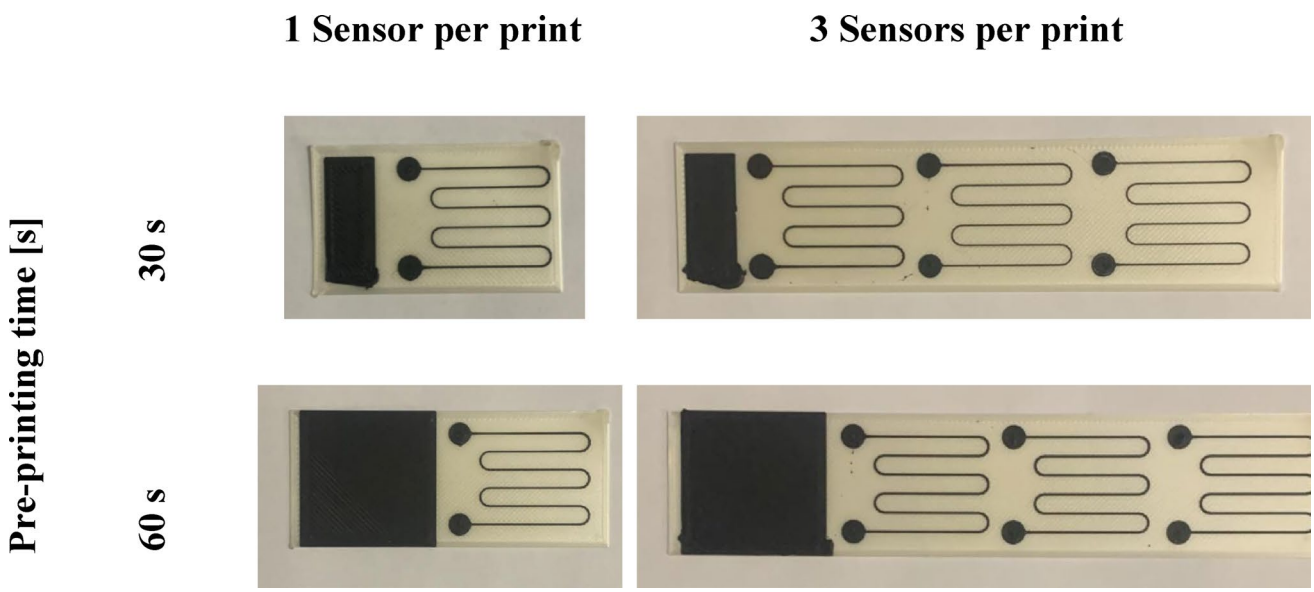

Fig. 4 The four setups for the preliminary test

result, any initial printing transient of the PLAc accounts for a significant portion of the total PLAc deposition. Moreover, the PLAc is maintained at both warm and hot standby temperatures during the process for two reasons. First, in the dual-material extrusion setup, each nozzle is held at a warm temperature during inactivity (128 °C for PLAc). Second, this approach accounts for the topography of the substrate onto which the PLAc is deposited. The sensor's electrical resistance depends on its cross-sectional geometry, which is influenced by the substrate's surface topography. The sensor's electrical resistance depends on its cross-sectional geometry, which is influenced by the topography of the substrate on which it is deposited. Therefore, a flat substrate surface is preferred to ensure a more uniform cross-section, simplifying measurement and comparison amongst the samples. An ironing step was thus used to flatten the top surface of the substrate where PLAc is deposited. The ironing process is a heat treatment used to smooth the surface of a printed layer. During ironing, the nozzle is heated at the extruding temperature of the material, and it moves all along the printed layer. Moreover, no material extrusion occurs. During the movement, it brushes and locally melts the polymer so spreading the material. As a result, a smoother layer surface is obtained. However, as the hot nozzle locally melts and smooths PLA, the temperature of PLAc is raised and kept at the extrusion value (Table 2) as long as ironing lasts. Given these aspects of the manufacturing process, preliminary tests were performed to evaluate their effects on the sensor characteristics.

Accordingly, two factors were examined: the substrate dimensions and the PLAc pre-print time, which serves to purge the nozzle and allow for stabilization before sensor printing. The substrate dimension determines how long PLAc is held at warm and high temperatures. Moreover, larger substrates enable printing multiple sensors in a row (Fig. 4), allowing assessment of any initial process drift caused by the printing transient. The PLAc purging was done by pre-printing a third part (a rectangle of PLAc, one layer thick, whose dimensions determine its printing time) before the sensor. Accordingly, the investigated factors were called "sensors pre-print" and "pre-printing time" (Table 3). Two substrate dimensions (N) were considered (i.e., able to hold 1 or 3 sensors plus the pre-printed material); two pre-printing times were chosen (30 ± 1 s and 90 ± 1 s, respectively), and the substrate surfaces were ironed. Each combination was repeated 3 times for a total of 12 prints and 24 samples. A nozzle cleaning procedure was performed every 3 samples (Table 3). Samples were further measured to evaluate actual cross-section and electrical resistance (R). The geometry of the sample cross-section was measured using the PF60 laser microscope (Mitaka™, Japan) and the software Mitakamap Premium (Mitaka™, Japan). The

Table 3 Experimental plan and classification for the preliminary test

Name	Pre-printing time [s]	Sensors per print	Ironing	Replicates	Nozzle cleaning
P_30_1	30	1	No	3	Every 3 samples
P_30_1_Iron			Yes		
P_30_3		3	No		
P_30_3_Iron			Yes		
P_90_1	90	1	No		
P_90_1_Iron			Yes		
P_90_3		3	No		
P_90_3_Iron			Yes		

electrical resistance of the sensors was instead measured using a standard multimeter model Powermeter KDM-360 CTF and its probe test leads. The lead tips were positioned at the very start and at the very end of the sensor, on the two circles (Fig. 3). Furthermore, the tips of the probes were laid down sideways to ensure a larger contact surface with the sensor. The measurements were carried out by the same person, applying constant contact pressure between test leads and sensor until the resistance value stabilizes. To assess the reliability of this measuring method (namely Pow-Tips), it was compared with two other methodologies. In particular, it was compared to the use of clip probes together with i) the previously mentioned KDM-360 CTF powermeter (namely Pow-Clips), and ii) the Impedance Analyser (MFIA Impedance Analyser Precision LCR Meter by Zurich Instruments, namely IAP-Clips). A total of 10 samples were printed, and the results of the three measuring methods were recorded and reported in Fig. 3, showing that the three methods are equivalent (p-value 0.978) with numerical scatter which ranges from − 1.6 to 0.7% (IAP-Clips is used as base-value for the comparison). Accordingly, the method KDM-360 CTF powermeter with probes (Pow-Tips) was preferred for its ease of use.

The cross-section of the sensor (Fig. 5a) was measured in width (w), thickness (t), and area (A). Data were collected by scanning each sensor along 3 equally spaced lines using a scanning speed of 20 µm/s and a pitch of 2 µm. Each line crosses 6 times the conductive profile (Fig. 5b) for a total of 18 cross-sections per sensor, for a total of 432 cross-sections. The scanned profile of the surface along each line was compensated using a 4th-grade polynomial function. The typical result for each scan is reported in Fig. 5c, where each peak of the profile corresponds to one cross-section of the sensor. Then, each cross-section was isolated and elaborated (Fig. 6). The width (w) and thickness (t) values were evaluated, and the rectangular area (A) of the cross-sections was estimated. Finally, the average values and standard deviations of w, t, and A were estimated (Figs. 7, 8), and the electrical resistance of the samples at rest (R_0) was measured in a controlled-temperature room at 21 °C and correlated to the cross-sectional area (A) of the sensor (Fig. 9).

The effects of pre-printing time and printing order on the cross-section of the sensor are reported in Figs. 7 and 8. Generally, these two variables influence their dimensions (t and w) and area (A) both in values and uniformity. Moreover, a crossed-alternated effect amongst the tested parameters and dimensions is observed. ANOVA tests on the thickness, width, and their standard deviation were performed over pre-printing time and sample. In particular:

- *Pre-printing time*. When the small substrate is considered (N = 1), the sensor thickness (t), Fig. 7, is not influenced by pre-printing time (p-value = 0.508), but its standard deviation (σ_t) is (p-value = 0.003). On the

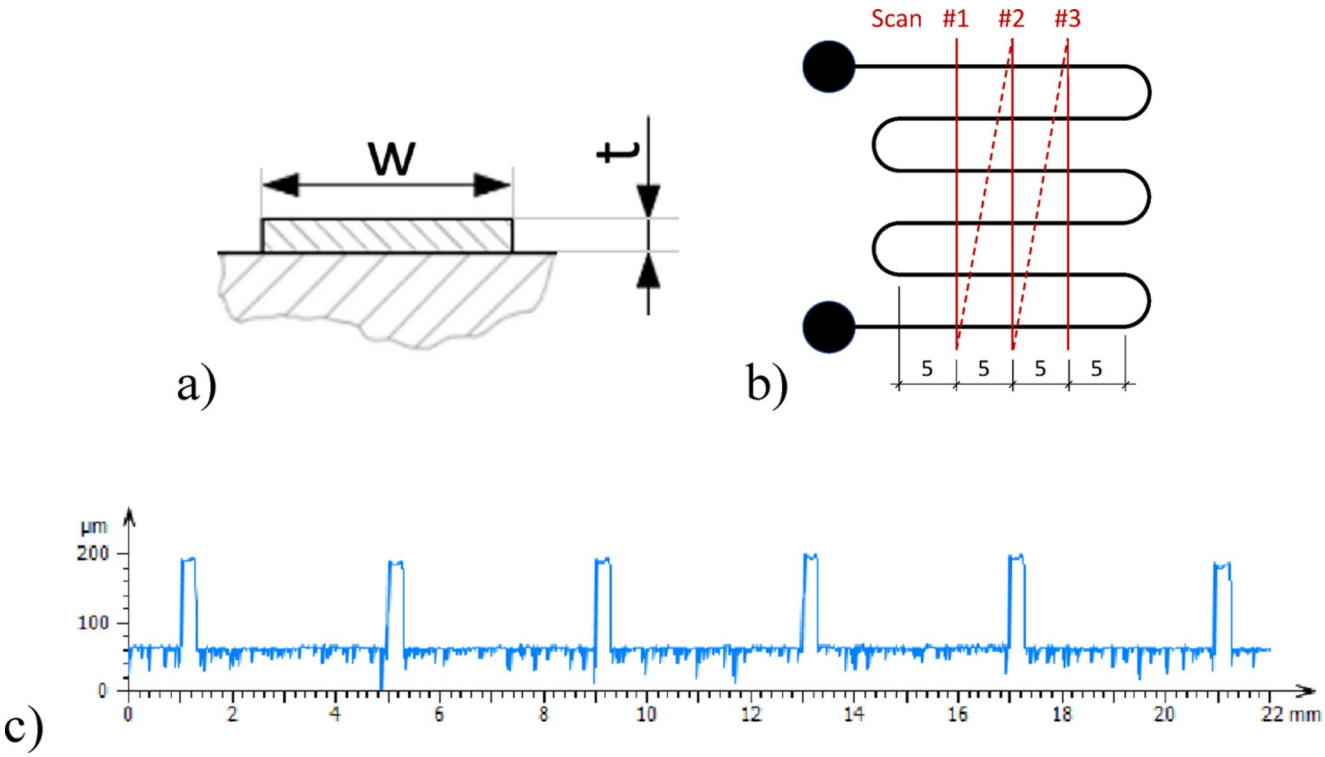

Fig. 5 Geometrical characterization of the samples. **a** Cross-section geometry, **b** scanning sequence, dimensions are in mm, and **c** profile detected along one scan

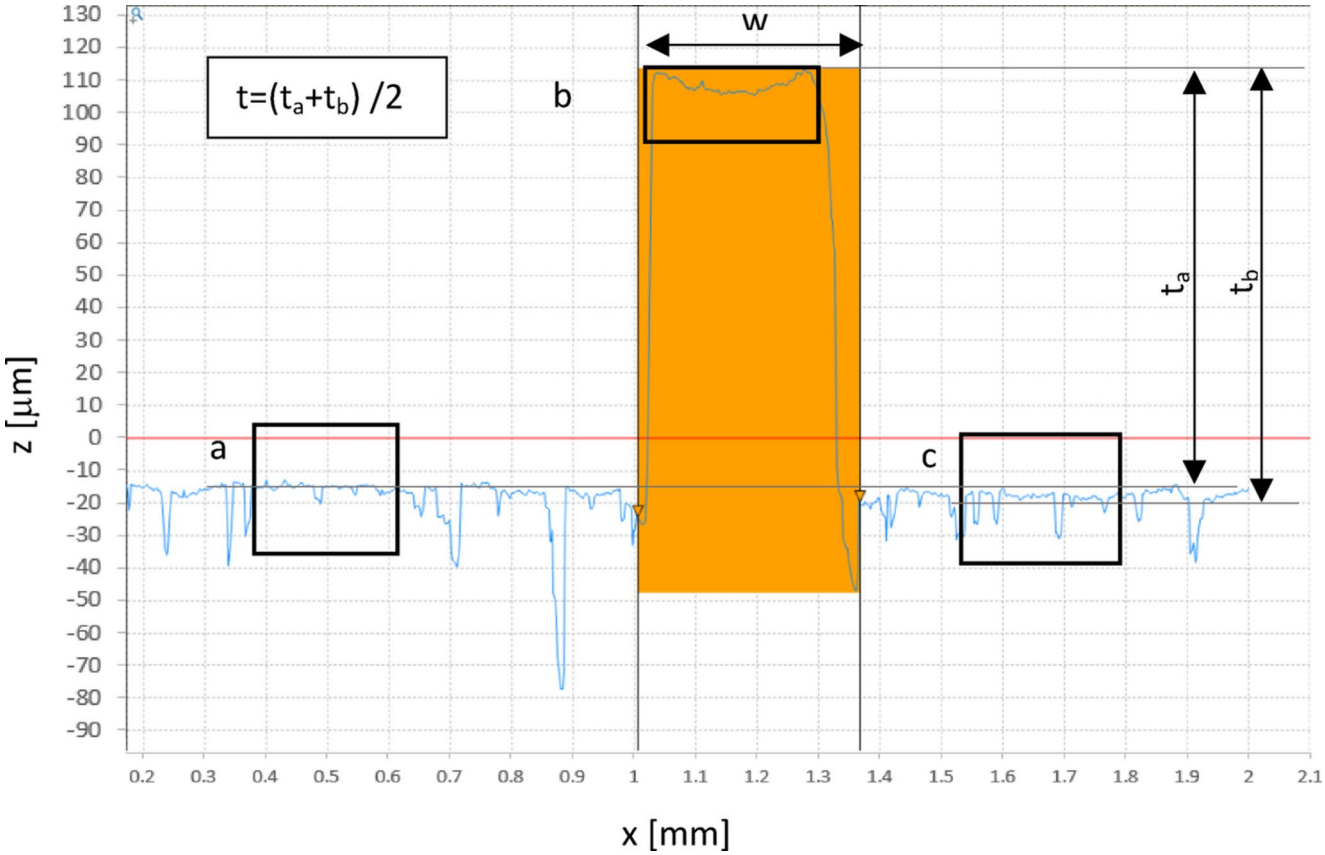

Fig. 6 Procedure for estimating width (w) and thickness (t) for each scanned cross-section. The graph shows the scanned profile of the sensor. The black lined rectangles, namely a and c, highlight the profile of the PLA substrate. The orange-filled rectangle, namely b, shows a local top-flattened peak, which is the cross-section of PLAc. The lateral sides of the peak are used to determine the width value (w). The thickness (t) is obtained as the mean of t_a and t_b. The values of t_a and t_b are obtained as the difference in height between the maximum peak height (b range) and the mean height of the substrate (a and c ranges)

contrary, the sensor width (w) decreases as pre-printing time rises (p-value = 0.027), but its standard deviation (σ_w) does not (p-value = 0.554). This is not present in larger substrates (N = 3), even though the sample thickness (t) is higher for sample = 1 (p-value = 0.001) than in smaller substrates (N = 1).

- *Sample printing order*. In large substrates (N = 3), the sample thickness (t) decreases with the print order (sample 1 to 3, p-value = 0.001), Fig. 7. This confirms that an initial transient is present during sensor printing, and sensors were printed during that transient time.

Given the alternated effects on t and w, the cross-section of the sensor was approximated with a rectangle, and its area (A) was considered a comprehensive estimator of the extrusion process (Fig. 8). The results reflect the trends of w and t in terms of both process drift and sensor uniformity. ANOVA tests on the cross-section and its standard deviation were performed over pre-printing time and sample. Indeed, the influence of pre-printing time on the cross section for N = 1 is confirmed. In particular, it influences both the area (A, p-value < 0.001) and its standard deviation ($\boldsymbol{\sigma}_A$, p-value = 0.003). Furthermore, the influence of the sample printing order is confirmed of both A (p-value = 0.003) and $\boldsymbol{\sigma}_A$ (p-value = 0.004). Accordingly, the electrical resistance of the sensors at rest (R_0) was correlated to the cross-sectional area (A), and the results (Fig. 9) showed an inverse correlation. Some data scattering is present, which is explained by the approximation of the cross-section as a rectangle and by the measuring method (laser scan from the top point of view), which does not allow for measuring the undercut profile of the cross-section of the sample.

Based on the correlation between the electrical properties of the sensor and the cross-section area, R_0 was used as an indicator of the PLAc extrusion process. In particular, by comparing the samples printed with and without ironing (Fig. 10), the results show that ironing influences the resistivity (R_0) of the sensor both in scattering and values. This is respectively confirmed by the test of equal variances (p-value < 0.001) and the Welch t-test (p-value < 0.001). Ironed surfaces have a higher average resistivity and,

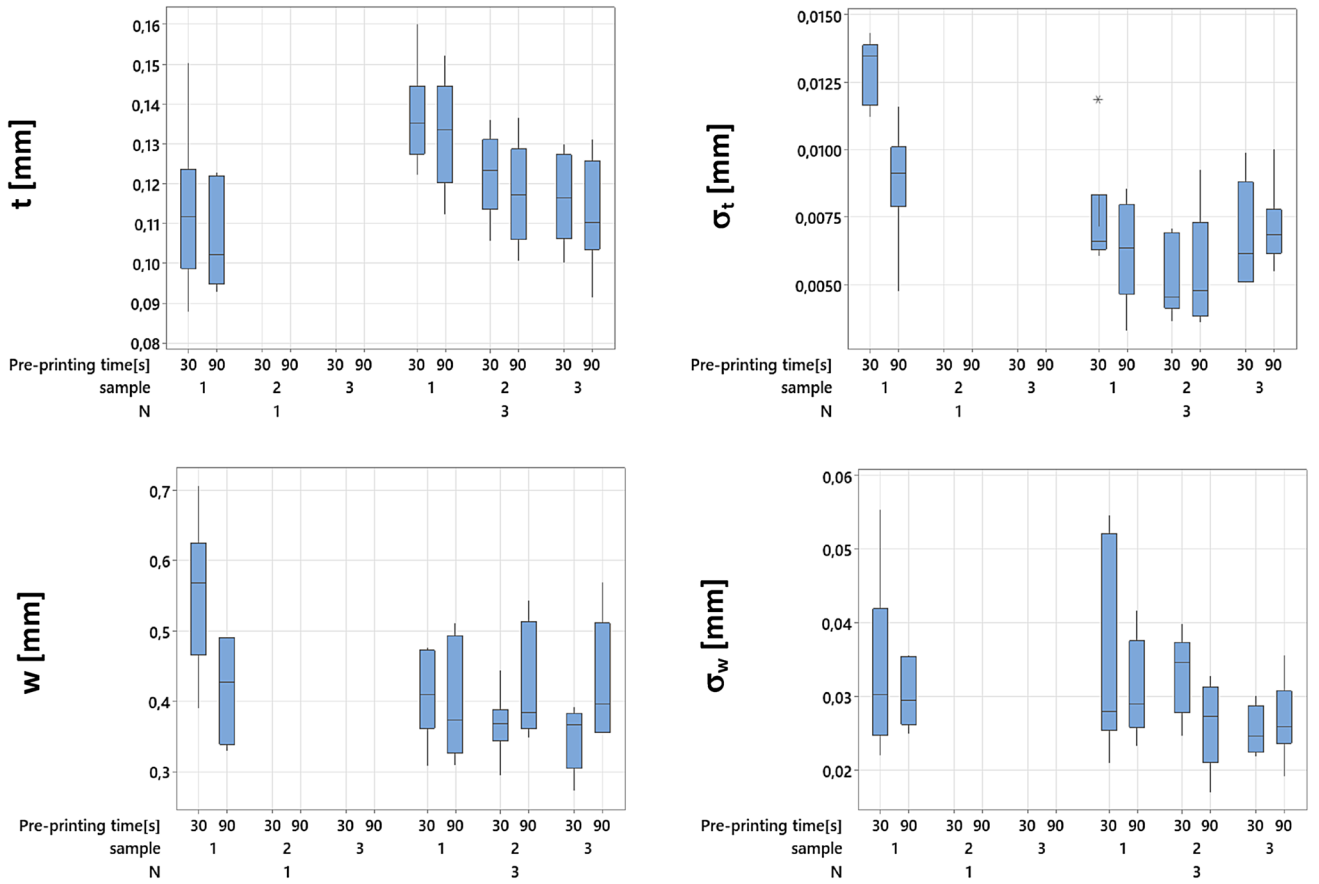

Fig. 7 Effects of pre-printing time, substrate dimension, and sample print order on each sample thickness (t) and width (w) of the sensor cross-section. Boxes represent the 2nd and 3rd quartiles, and vertical lines indicate the range

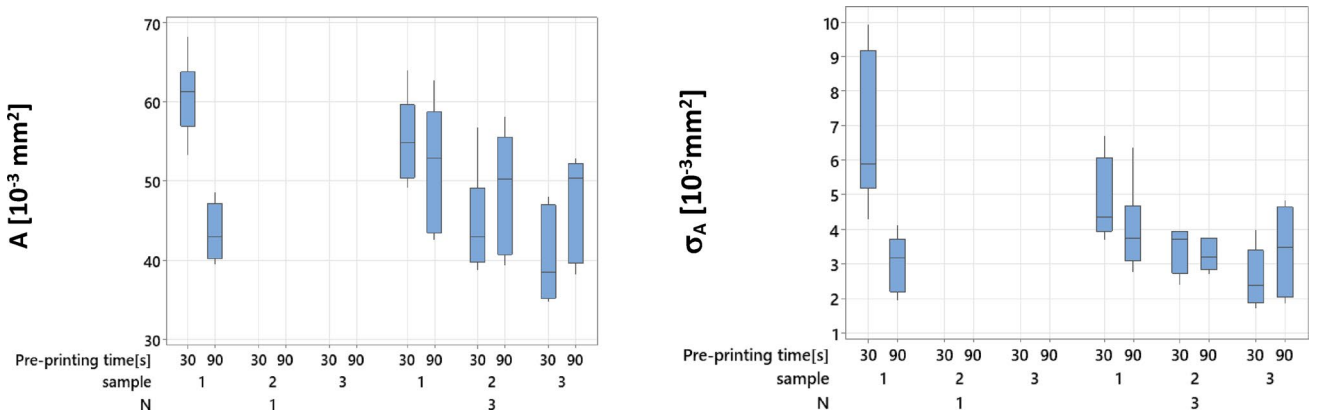

Fig. 8 Effects of pre-printing time, substrate dimension, and sample print order on cross-section area (A) of the sensor cross-section. Boxes represent the 2nd and 3rd quartiles, and vertical lines indicate the range

therefore, are more sensitive, but a non-ironed substrate leads to less scattered R_0 values.

Overall, the following considerations can be drawn from the preliminary tests.

- *R_0 as an index of the process*. The correlation between R_0 and A allows the use of the sensor's electrical resistance as an indirect measure of the material deposited by the process (Fig. 9). Moreover, the measure of R_0 is coherent with the strain gauge nature of the sensor. Additionally, its measurement allows rapid feedback on the process compared to the scanning and elaboration times required by t and w measurements.

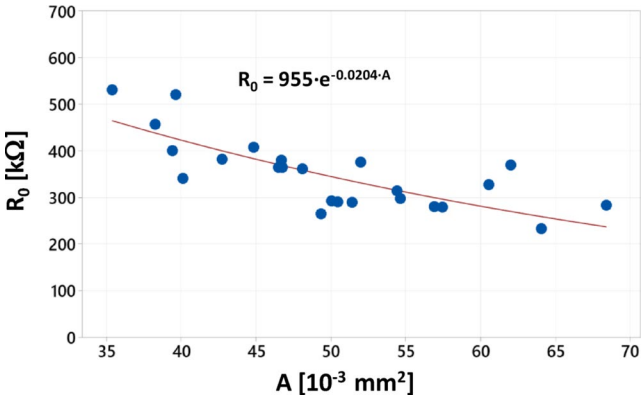

Fig. 9 Correlation between the electrical resistance at rest (R_0) and the mean cross-sectional area (A) of the sample

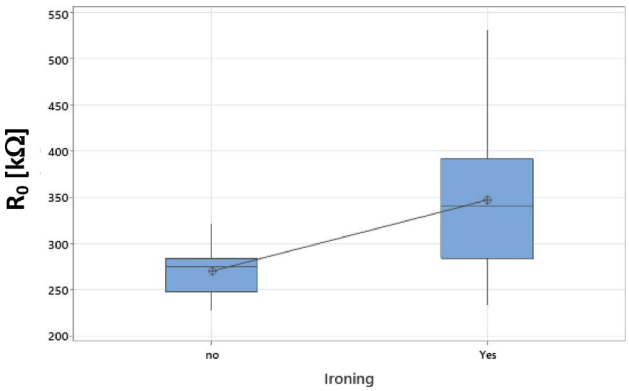

Fig. 10 Effect of substrate ironing on the electrical resistance of R_0. Boxes represent the 2nd and 3rd quartiles, vertical lines indicate the range, and connection lines refer to the average values of the groups

- *No Ironing*. Ironing was adopted to deposit PLAc on a smoother surface and enhance the cross-section uniformity as its dimensional analysis. The results show that R_0 can be a substitute for A, indicating that ironing is not further required. Moreover, ironing makes the process less repeatable. Therefore, it is preferable to avoid substrate ironing.
- *Effect of standby temperature.* The effects of the pre-printed material on the cross-sectional area (A) of the sensor show that a larger and more variable volume of material is initially extruded (results for N = 1 in Fig. 8), which becomes lower and more uniform when more material is pre-extruded. Instead, when a wider substrate is used (results for N = 3 in Fig. 8), the pre-printed material effect is irrelevant. These behaviours are attributed to the standby temperature of PLAc during the process.In particular, Zhang et al. [42] demonstrated the existence of a temperature gradient in the extruding filament. The temperature decreases from the outer part of the filament to the core during extrusion, and its gradient depends on the material flow rate. As the flow rate decreases, the gradient reduces, and the average extrusion temperature rises. Accordingly, during stand-by temperature, the flow rate is zero, the material is therefore overheated, and it is extruded at a higher temperature during the subsequent printing. This leads to the initial over extrusion of material observed in Fig. 8. Then, as new and cold material flows through the nozzle, the extrusion temperature reaches the standard condition together with the deposited cross-section area (A). This phenomenon is more important in wider substrates because ironing requires more time and, consequently, PLAc remains longer at high standby temperatures. Accordingly, the relief effect of the pre-printed material was more effective for smaller substrates, which involves shorter stan-by time for PLAc.
- *Process initial transient*. When printing a sequence of samples (results for N = 3 in Fig. 8), a drift of the cross-section (A) values can be observed. This confirms the presence of an initial extrusion transient, likely caused by the standby temperature, as previously discussed, and the nature of the MEX process itself. The evidence of a steady state of the process is also not visible in the results. This indicates that most, if not all, of the sensors produced in these preliminary tests were printed during the initial process transient.

2.3 Experimental campaign

A second experimental campaign was conducted to characterize and optimize the sensor printing process, with a focus on improving repeatability. Higher values of pre-printing time and a longer sequence of sensors were considered to identify the most stable process conditions.

Tests were conducted: 4 values of pre-printing time (30, 90, 180, and 330 s) and 12 sensors printed on the same substrate (Fig. 11a). Every test was replicated 3 times for a total of 144 sensors printed (Table 4). Based on the previous considerations, results were compared using the sensor electrical resistance (R_0, Fig. 9). Moreover, the substrate ironing step was no longer adopted since sensors with that heat treatment resulted in more variable (Fig. 10).

The results in Fig. 11b show that R_0 depends on the printing order of the sample, and it has an oscillatory profile in values and scattering. This is a consequence of the printer temperature control switching the heating cartridge of the nozzle alternatively on and off, affecting the amount of material extruded and, contextually, the cross-sectional area of the electrical resistance.

Within this variability amongst the test conditions and along the printing sequence, data were statistically analysed using ANOVA. An initial attempt was made to analyse the entire data set as a single experimental design, but no consistent results were obtained. In fact, regardless of the

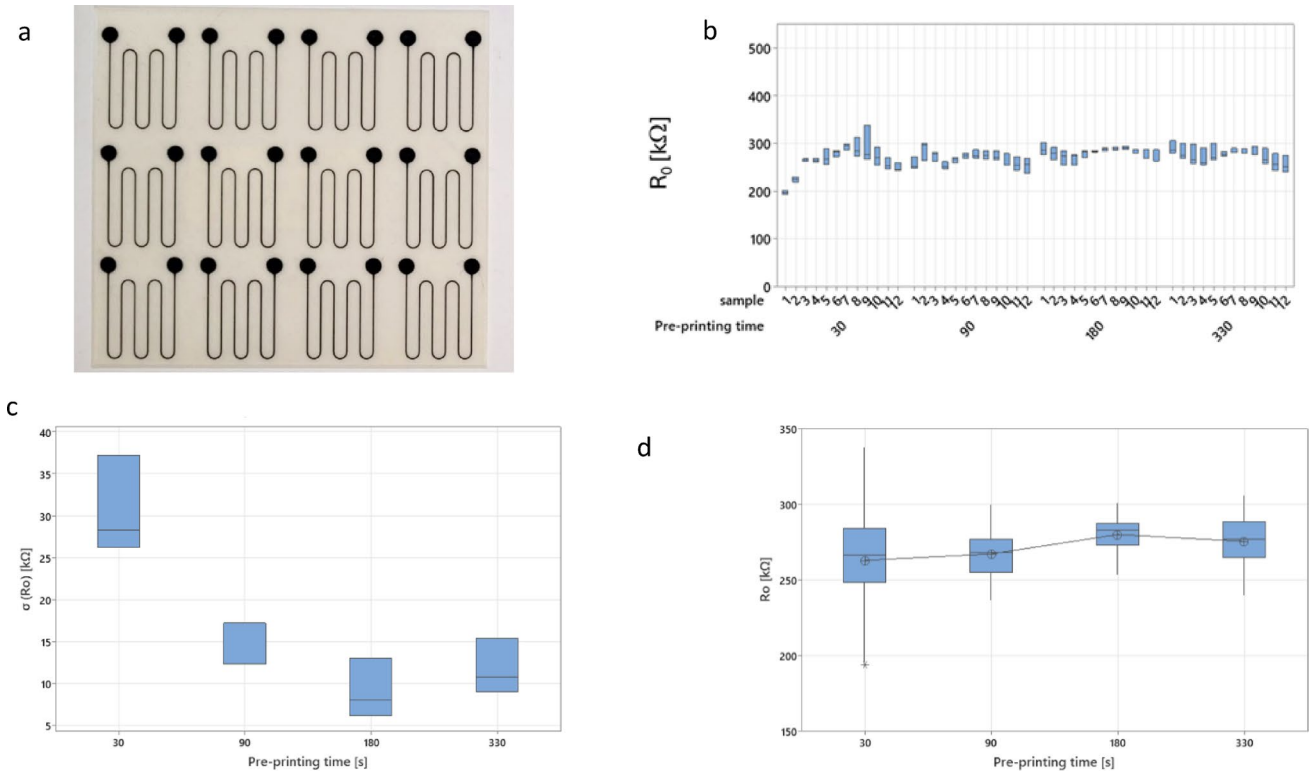

Fig. 11 Experimental tests: Printed samples and electrical resistance (R_0) profile as pre-printing time and printing order change. Boxes (in b, c, and d) represent the 2nd and 3rd quartiles, vertical lines indicate the range, and connecting lines refer to the average values of the groups

Table 4 Tests conducted in the experimental campaign

Name	Pre-printing time [s]	Sensors per print	Ironing	Replicates	Nozzle cleaning
P_30_12	30	12	No	3	Before each printing
P_90_12	90				
P_180_12	180				
P_330_12	330				

regression model adopted (factorial designs, response surface, or general regressions), the residuals were found to be neither normal nor independent. Therefore, a step-by-step analysis was performed to identify subsets of process conditions that lead to a more repeatable printing process. Initially, the uniformity of samples within the same print batch was taken into consideration. In particular, the standard deviation of the resistance (σ_{Ro}) of the 12 sensors was estimated and analysed as the pre-printing time varies (Fig. 11c). ANOVA results show that pre-printing time influences variability within the print batch (p-value = 0.001). Moreover, groups 90 to 330 s are similar (p-value = 0.262), resulting in more uniform batches. Then, the electrical resistance (R_0) was analysed for these groups (Fig. 11d), and regression analysis confirmed the influence of pre-printing time and sample print order (p-value < 0.001 for both). Conversely, if the analysis is limited to the 180 and 330 s groups, only the sample printing order determines the sensor resistance (p-value = 0.003), while the pre-printing time is not significant (p-value = 0.172). Finally, using 180 s and 330 s, the first printed samples (3 replicates each) have similar R_0 values (p-value = 0.793). These results demonstrate that a pre-printing time of 180 s is sufficient to eliminate the effects of standby temperature. Furthermore, the variability of the sensor resistance (R_0) is due exclusively to process fluctuations (Fig. 11b).

Accordingly, 180 s should be adopted to reach the steady state of the process, and one sensor per time should be printed to avoid the effect of the temperature control. The summary of the process parameters that were identified to print strain-gauge resistive sensors made of Protopasta™ conductive PLA (PLAc) is reported in Table 5.

3 Flex sensor characterisation

The sensor's flex behaviour was assessed by measuring its resistance at rest and when bent. In particular, static (Fig. 12a) and cyclic tests (Fig. 12b) were performed.

Table 5 Summary of the printing process of Protopasta™ conductive PLA (PLAc) filament for fabricating strain-gauge resistive sensors

Parameters	Value	Units
Layer height (h)	0.15	[mm]
Temperature (T)	220	[°C]
Printing speed (v)	25	[mm/s]
Flow rate	100%	
Line width	0.45	[mm]
PintCore	AA0.4	
Pre-printing time	180	[s]
Substrate ironing	No	
Sensors per print	1	

3.1 Static bending tests

Bending tests were performed using two metal cylinders with curvature radii (R_b) of 30 mm and 60 mm, respectively, with the sensors secured to the curved surfaces using elastic bands (Fig. 12a). Sensor resistance was measured at rest (R_0) and when bent (R_b). Moreover, their Gauge Factor (GF) was estimated. Bending tests were performed on the samples previously printed on strips together with new sensors (Table 6). A total of 16 additional sensors were singularly printed according to the results of the process optimisation (Table 5). The nozzle was cleaned only before the first sensor printing.

Table 7 reports the results of the tests. The average value ($\overline{R_0}$) and standard deviation (σ_{Ro}) of the resistance at rest amongst the replicates confirm the influence of the printing process. Sensors are more uniform (i.e., lower σ_{Ro} values) when 1 sensor is printed at a time without ironing. Moreover, the tests conducted using the optimal process

Table 7 Effects of the printing parameters on the printed sensors. Resistance at rest (mean value $\overline{R_0}$ and standard deviation σ_{Ro}) and linear correlation coefficient (mean value $\overline{R^2}$ and variance σ_R^2) of the response under constant curvature (1/r) bending

Name	Resistance at rest (kOhm)		Linear correlation: $R_b = f(1/r)$	
	$\overline{R_0}$	σ_{Ro}	coeff.$\overline{R^2}$	σ_R^2
P_30_1_Iron	341	82	0.996	0.005
P_30_3_Iron	327	35	0.997	<0.001
P_90_1_Iron	341	60	0.987	<0.001
P_90_3_Iron	431	66	0.990	0.009
P_30_1	243	11	0.992	<0.001
P_30_3	274	31	0.964	0.003
P_90_1	272	13	0.994	<0.001
P_90_3	284	17	0.988	<0.001
P_180_1	229	14	0.994	<0.001

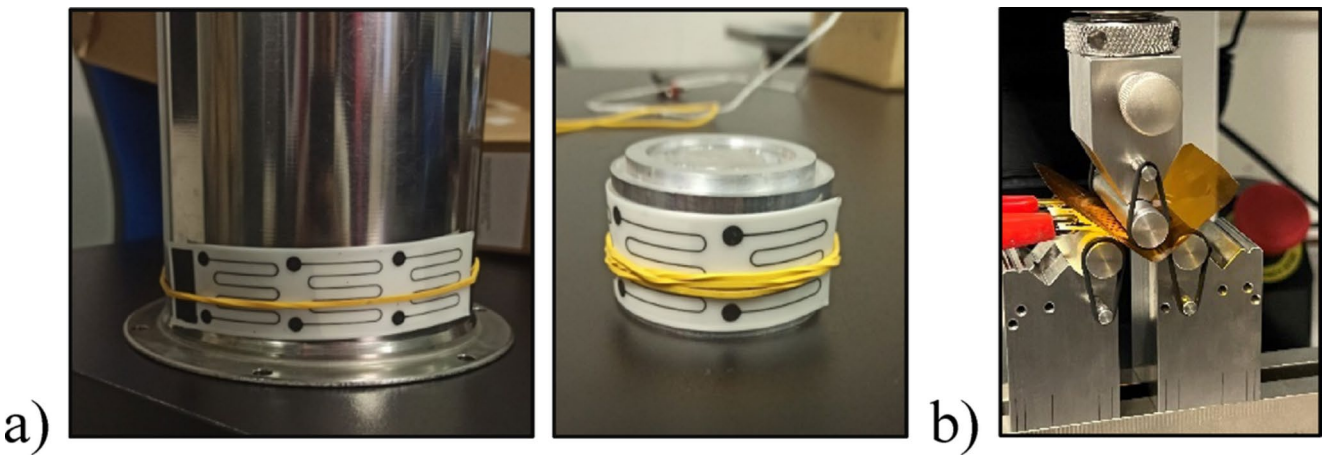

Fig. 12 Flex characterisation setup for r = 60 mm and r = 30 mm (**a**); setup of the bending test carried out using the dynamometer, 10 cycles of deformation were performed setting the maximum displacement at 4.5 mm and the speed at 0.75 mm/s (**b**)

Table 6 Summary of the sensor flex tests

Test name	Pre-printing time (s)	Sensors per print	Ironing	Replicates	Nozzle cleaning	Curvature radii (mm)
P_30_1_Iron	30	1	Yes	3	Every 3 samples	0–30–60
P_30_3_Iron		3				
P_90_1_Iron	90	1				
P_90_3_Iron		3				
P_30_1	30	1	No			
P_30_3		3				
P_90_1	90	1				
P_90_3		3				
P_180_1	180	1		16	Every 16 samples	

conditions reported in Table 5 (i.e. ", *P_180_1"*) demonstrate that repeatability is achieved in low- to medium-sized batches of sensors (16 in this case).

Figure 13 shows the trend for R_b over R_0 (for both the bending radii) and some examples of the sensor response (ΔR) when bent with constant curvature (estimated as r^{-1}). In the first graph is displayed that the behaviour of Rb over R0 is linear, for both the radii ($R^2=0.98$ for r=30 mm, and $R^2=0.95$ for r=60 mm). Amongst the "*P_180_1"*, 6 were selected in the whole span of "*P_180_1"* results to show that the behaviour of the sensors is linear while their sensitivity (i.e., the slope) is variable (Fig. 13b). The linearity of these sensors is confirmed by Table 7, which reports the average value ($\overline{R^2}$) and standard deviation ($\sigma_R{}^2$) of the linear regression coefficients for each group of replicates. In particular, the sensors printed with the optimal parameters in Table 5 (i.e., "*P_180_1"* test) showed linearity with $\overline{R^2}=0.994$ and $\sigma_R{}^2<0.001$.

The sensitivity of the tested strain train gauges was evaluated using the Gauge Factor (GF) according to Eq. 1. In particular, ΔR was calculated as the difference between the bent resistance (R_b) and the resistance at rest (R_0); experimental values of the resistances (R_0 and R_b) were used (Fig. 13a). The deformation ε was estimated as the ratio between the elongation (ΔL) and the initial length (Lo) of the sensor Eq. 2.

$$GF = (\Delta R/Ro)/\varepsilon \tag{1}$$

Equation 1: Gauge factor definition

$$\varepsilon = \frac{\Delta L}{Lo} \tag{2}$$

Equation 2: strain definition.

The estimation of ΔL was done assuming that the deformation (for both substrate and sensor) is continuous and linear across the printed layers (Fig. 14). Moreover, the bent sample is compressed at the intradoss (i.e., bottom layer of the substrate) and stretched at the estradoss (i.e., upper surface of the sensor). Given the continuity, one undeformed surface (the neutral fibre, NF) is located between these two surfaces. Its position is not known, but linearity and continuity locate the NF at half of the sample total height (H). Within these assumptions, the strain (ε) within the sample can be expressed as in Eq. 3, where z is the coordinate along the thickness, Rb is the bending radius, and H is the total height of the sample.

$$\varepsilon = \frac{2z}{2R_b + H} \tag{3}$$

Equation 3: Strain as function of the distance from the NF.

The PLAc sensor has a finite height (h); therefore, its deformation is not constant along the z-axis. Given the linearity assumption, the average value of its deformation (ε) was estimated at half of the sensor height. Being the total thickness of the sample, H=0.6 mm, and the thickness of the sensor h=0.15, the sensor deformation was estimated at z=0.225 mm. Accordingly, the strain gauge deformations are $7.46\cdot10^{-3}$ and $20.2\cdot10^{-3}$ for R_b=60 mm and R_b=30 mm, respectively.

Then, the GF was estimated for the tested samples and analysed. Results showed that the GF of the sensor is independent from the tested bend radii (*p*-value=0.987), the values are normally distributed (*p*-value=0.231) with average and standard deviation values of 14±2.3. Literature reports a gauge factor between 2 and 4 for commercial metal sensors

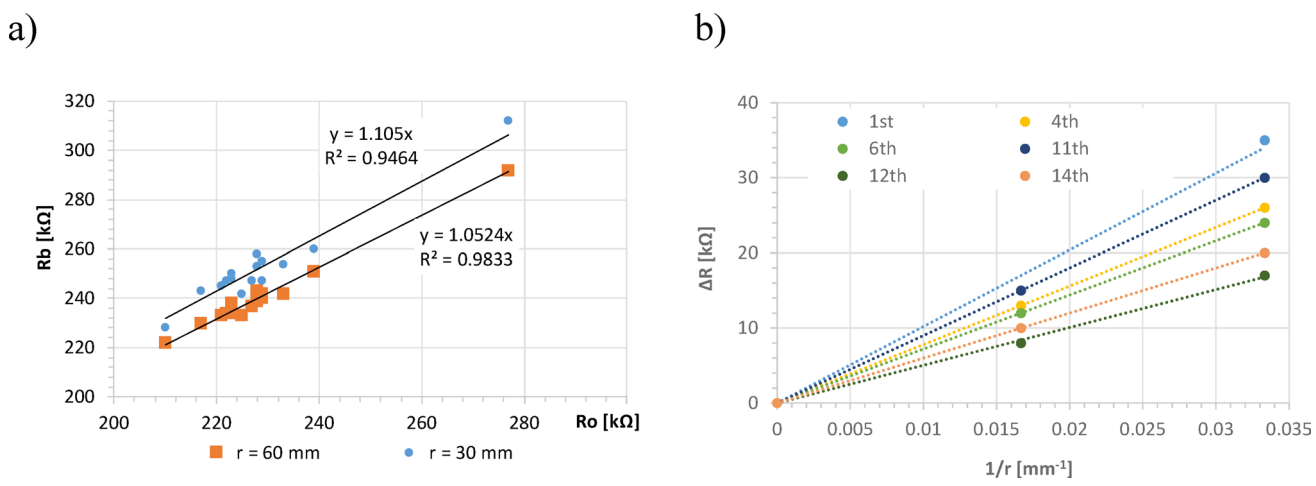

Fig. 13 Variation of the electrical resistance of the sensors during constant curvature bending. R_b over R_0 shows a linear correlation for both bending radii (**a**). In the second graph (**b**) the results reported belong to the group of tests "P_180_1" and cover the entire span of the group results; the run order is shown in the caption

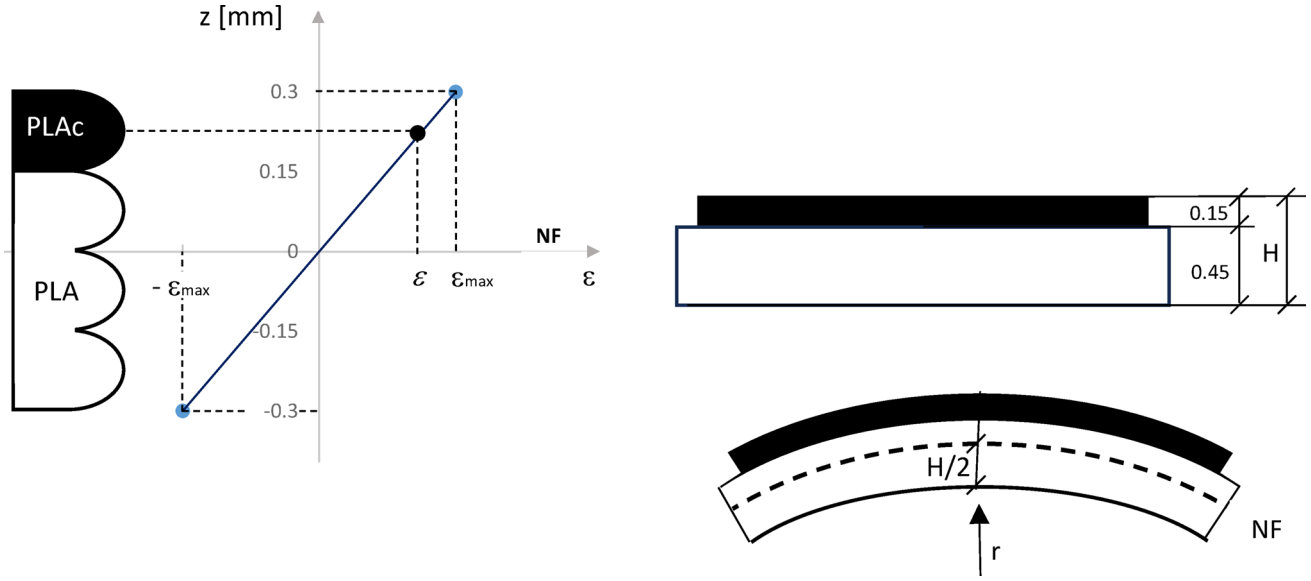

Fig. 14 Graphical illustration of the approach followed to calculate the strain: which was calculated at half the height of the PLAc layer, considering a linear trend between the distance from the neutral fibre and the strain itself. The neutral fibre was considered at half of the total sample height (H)

[43] and between 80 and 200 (absolute values) for semiconductors [43, 44]. Therefore, the developed sensors have a sensitivity comparable to but significantly higher than metal strain gauges.

3.2 Cyclic bending tests

The cyclic behaviour of the sensor was tested under 3-points bending conditions. In particular, the dynamometer DC4050 by MARK-10 (Fig. 12b) was used to bend the sample; the ram of the dynamometer moved at 0.75 mm/s with a maximum displacement of 4.5 mm. The sample was poisoned with the strain gauge positioned towards the inner curvature surface of the substrate. A total of 10 bending cycles was tested. During the test, the electrical resistance of the sample was measured using an Impedance Analyser (MFIA Impedance Analyser Precision LCR Meter by Zurich Instruments). Figure 15a, b report the typical profile of the electrical resistance of the sensor as the ram moves. In particular, the resistance decreases with displacement up to around 1.5 mm. For bigger displacements, the resistance increases again until the maximum displacement (4.5 mm) is reached. Then, as the displacement reduces again, the resistance also reduces until the displacement is around 1.5 mm, and increases again up to 0.5 mm displacement, and then decreases again. Figure 15c shows the overall behaviour along the 10 cycles; in particular, the values of the sensor resistance undergo a settling phase and stabilise around the 7th-8th cycle.

4 Case study

The Simon™ electronic game from the 80 s was built using sensors FFF printed with the optimal parameters obtained in Table 5 [45]. Different from the original game, which uses on/off buttons, the present game uses the strain-gauge sensors together with an electrical resistance threshold value. A publicly available version of the game code [46] was adapted to function with resistive buttons and then uploaded to an Arduino® Uno Nano board. Specifically, one resistor (100 kΩ) is connected in series with the strain-gauge to obtain a voltage divider. Accordingly, the software estimates the resistance of the sensor, and it records the press action when the button is bent over the threshold value (300 kΩ). The electrical diagram designed in Thinkercad is shown in Fig. 16.

The strain gauges used have the same total length as the previous samples but are half the height and feature twice the number of curves. Additionally, they are fully enclosed in a PLA case to provide insulation and protection against wear (Fig. 16). Wires are connected to the sensors by mechanical interference.

The outcome is a device customisable in dimension, key stiffness, and sensor sensitivity that could be used in personalised medicine to train and strengthen the hand and fingers, as explained in the conclusions.

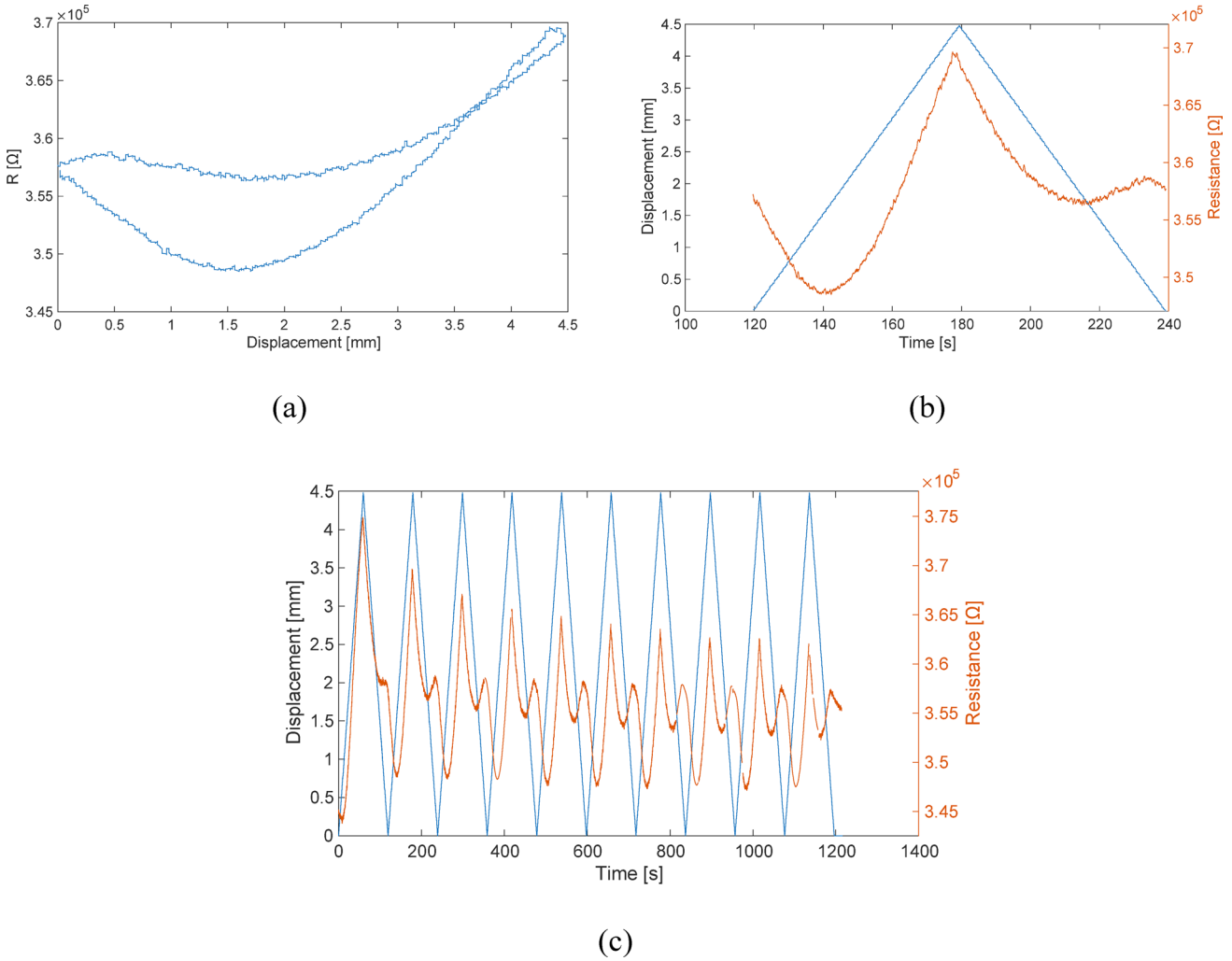

Fig. 15 Trend of resistance over displacement for the second cycle, the values were collected using the dynamometer with a maximum displacement of 4.5 mm at a speed of 0.75 mm/s (**a**). Focus on the behaviour of resistance and displacement in time for the second cycle (**b**). Overall trend of resistance and displacement over time for all 10 cycles (**c**)

5 Conclusions

AM MEX technology is recognized for its relatively low cost, broad material compatibility, and wide variety of applications. It is typically used to print large parts, whereas very small, fast-to-print components are less commonly produced. This is the case of the resistive strain-gauge sensors, whose manufacturing process and behaviour were investigated in the present work.

The investigation was carried out in successive steps to address the critical elements of short-time printing and to outline a robust process for managing them. Experimental tests revealed that factors such as the material stand-by temperature, the initial extrusion behaviour through the nozzle, and fluctuations in nozzle temperature caused by the heating system significantly affect the amount of material extruded. In particular, the effects of standby temperature and extrusion assessment are predominant at the beginning of the layer deposition. Furthermore, the nozzle temperature fluctuation is reflected by a wave-like behaviour of the material extrusion flow at a steady state.

In large and massive prints, these aspects may be negligible since local inhomogeneities can be spread around the part volume (i.e., randomising the layer sealing points), hence obtaining a macroscopically homogeneous part. On the contrary, very small parts are strongly affected by these phenomena since they are mostly or fully printed during the initial transient of the process, and the fluctuation period of the material flow can be longer than the part print time. Consequently, their geometry and properties are variable, as in the case of the PLAc sensors developed in the present research.

Accordingly, a printing protocol was developed to handle the process characteristics. The protocol mainly consists of

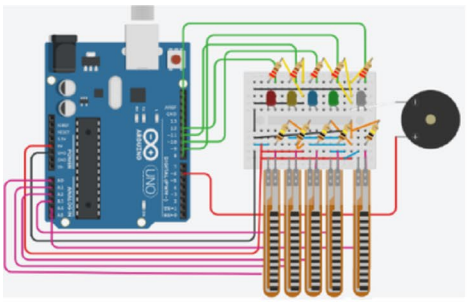

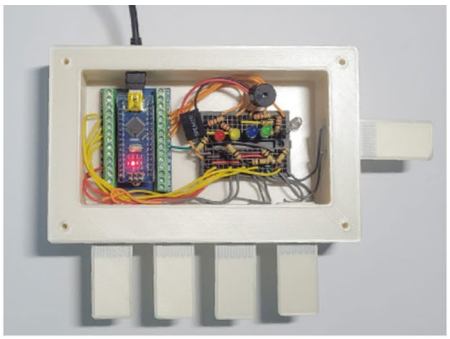

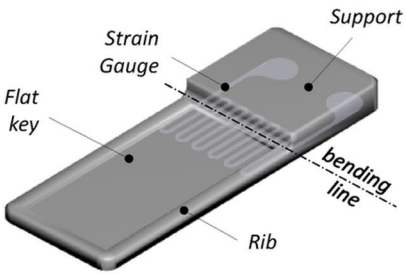
Support
Strain Gauge
Flat key
bending line
Rib

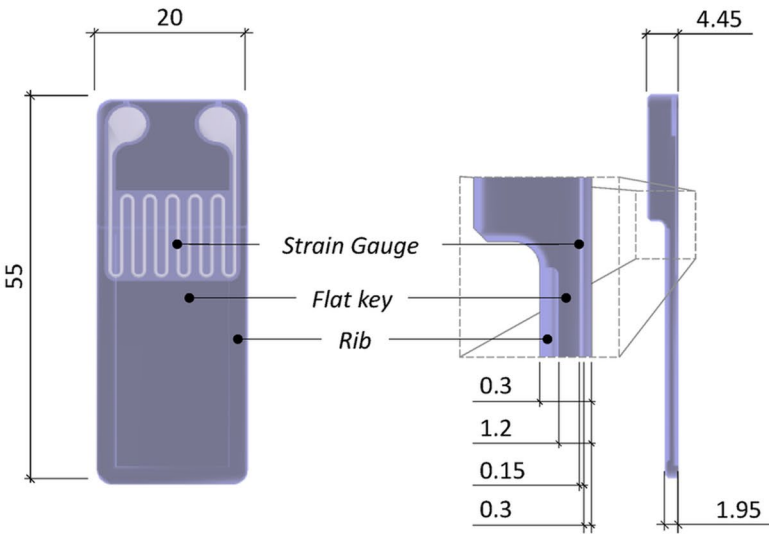
20
4.45
55
Strain Gauge
Flat key
Rib
0.3
1.2
0.15
0.3
1.95

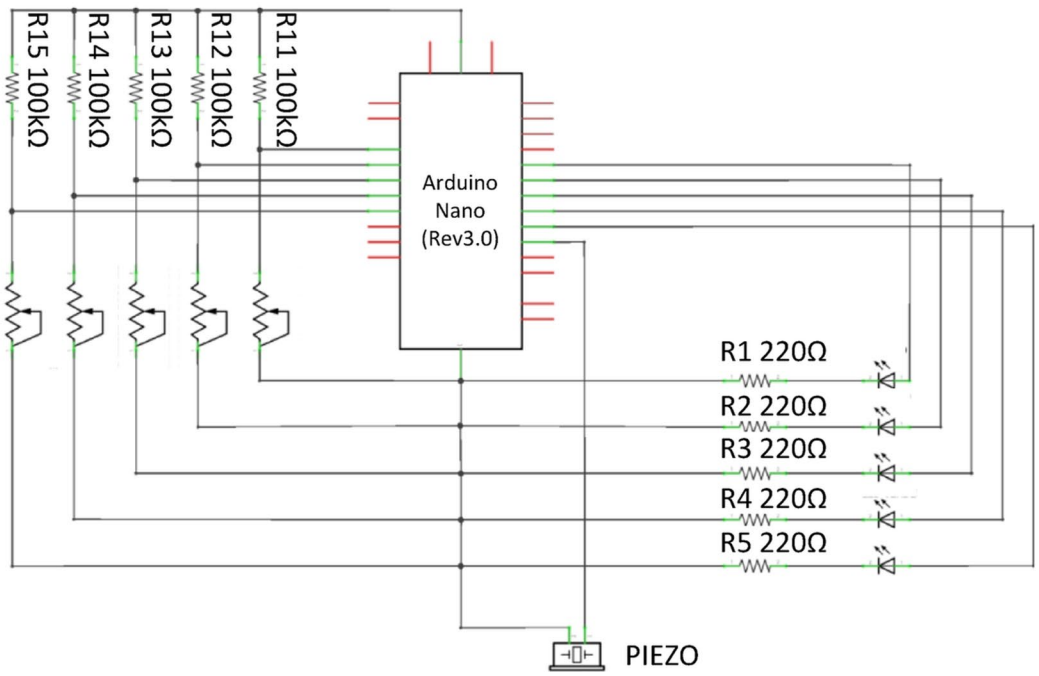
R15 100kΩ
R14 100kΩ
R13 100kΩ
R12 100kΩ
R11 100kΩ
Arduino Nano (Rev3.0)
R1 220Ω
R2 220Ω
R3 220Ω
R4 220Ω
R5 220Ω
PIEZO

Fig. 16 Device appearance, measurements, and electrical setup: assembled circuit, the front sight of the keys, and the back sight of the keys, dimensions in mm

a pre-printing period during which the PLAc material is extruded until the process transient is over. A pre-printing time of 180 s is sufficient for the Protopasta™ conductive PLA, as reported in Table 5. Moreover, one sensor at a time should be printed to avoid the effects of the fluctuating nozzle temperature, thus enhancing the homogeneity amongst the sensors. In these conditions, a batch of 16 strain-gauges with an average resistance of $\overline{R}_0 \pm \sigma = 284 \pm 14$ kΩ was obtained.

Under flex conditions, MEX printed sensors have a strong linear response in electrical resistance when bent with a constant curvature up to a 60 mm radius. Despite improvements in process uniformity, the response slope varies among the printed sensors. This affects the sensitivity of each FFF printed sensor but not their overall usability, indicating that they can still function effectively as flex sensors after initial characterization. Factors like substrate bending and bonding with the sensor material are instead significantly affecting the linear behaviour span. Further improvements may be achieved by optimizing the substrate, such as refining its topography. Moreover, the cyclic testing showed that the values of the sensor resistance undergo a settling phase and stabilise around the 7th-8th cycle. Therefore, to ensure a stabilisation in resistance values, it is suggested to consider a stage with some bending cycles before putting in use the sensor.

As a case study, final embedded strain-gauges were exploited for the fabrication of a working rhythm game customisable in dimensions, key stiffness, and sensor sensitivity. Such a device has potential in applications related to personalised medicine, aiming at training and strengthening the hand and fingers during patient rehabilitation. Sensor dimensions can be tailored according to the user's features (hand measurements and shape) and to the specific manual skills. The actual design uses flexible keys that need a small push to bend, being also suitable for patients with limited manual force. Keys' stiffness can be modified in length, thickness, or geometry to increase sensibility. During physical therapy exercises, gradually increasing the stiffness of the keys could be highly beneficial as the patient regains finger strength.

Therefore, MEX printed strain gauges offer a fast, low-cost, and customizable sensing solution that can be embedded into many components, providing significant benefits for smart objects and smart factory applications.

Supplementary Information The online version contains supplementary material available at https://doi.org/10.1007/s40964-025-01426-5.

Acknowledgements Authors want to sincerely thank Andrea Sbarra for working at the demonstrator. The authors also aknowledge Eng. A. Epicoco (Tec-Mec, UNIBS), and MICS (Made in Italy – Circular and Sustainable) Extended Partnership (Next Generation EU (Italian PNRR – M4 C2, 1.3–D.D.1551.11–10–2022, PE00000004 CUP D73C22001250001) for the electromechanical tests. The authors would like to aknowledge Prof. Elisabetta Ceretti (Department of Mechanical and Industrial Engineering, University of Brescia) for her general supersion in the project.

Author contributions A.F. and G.G. conceived and planned the research and workflow. G.G. and M.S. performed the tests, collected the data, and wrote the main manuscript text. A.F supervised the work and reviewed the manuscript. All authors reviewed the manuscript.

Funding Open access funding provided by Università degli Studi di Brescia within the CRUI-CARE Agreement.

Data availability Data is provided within the manuscript. If more detail is needed, Data will be made available upon request.

Declarations

Competing interests The authors declare no competing interests.

Open Access This article is licensed under a Creative Commons Attribution 4.0 International License, which permits use, sharing, adaptation, distribution and reproduction in any medium or format, as long as you give appropriate credit to the original author(s) and the source, provide a link to the Creative Commons licence, and indicate if changes were made. The images or other third party material in this article are included in the article's Creative Commons licence, unless indicated otherwise in a credit line to the material. If material is not included in the article's Creative Commons licence and your intended use is not permitted by statutory regulation or exceeds the permitted use, you will need to obtain permission directly from the copyright holder. To view a copy of this licence, visit http://creativecommons.org/licenses/by/4.0/.

References

1. Frohn-Sörensen P, Geueke M, Tuli TB et al (2021) 3D printed prototyping tools for flexible sheet metal drawing. Int J Adv Manuf Technol 115:2623–2637. https://doi.org/10.1007/s00170-021-07312-y
2. Frohn-Sörensen P, Geueke M, Engel B et al (2022) Design for 3D printed tools: mechanical material properties for direct polymer additive tooling. Polymers (Basel) 14:1694. https://doi.org/10.3390/polym14091694
3. Kong JS, Kim JJ, Riva L, Ginestra PS, Cho D-W (2024) In vitro three-dimensional volumetric printing of vitreous body models using decellularized extracellular matrix bioink. Biofabrication 16(4):045030. https://doi.org/10.1088/1758-5090/ad6f46
4. Hussan KSJ, Subramaniam MP, Kenz KTM et al (2024) Fabrication and challenges of 3D printed sensors for biomedical applications-comprehensive review. Results Eng 21:101867. https://doi.org/10.1016/j.rineng.2024.101867
5. Remaggi G, Zaccarelli A, Elviri L (2022) 3D printing technologies in biosensors production: recent developments. Chemosensors 10:65. https://doi.org/10.3390/chemosensors10020065
6. Rocha Neto JBM, Soares JC, Longhitano GA, Coatrini-Soares A, Carvalho HF, Oliveira ON Jr., Beppu MM, da Silva JVL (2022)

Three-dimensional printing and its potential to develop sensors for cancer with improved performance. Biosensors 12(9):685. https://doi.org/10.3390/bios12090685
7. Korelidou A, Domínguez-Robles J, Magill ER et al (2022) 3D-printed reservoir-type implants containing poly(lactic acid)/poly(caprolactone) porous membranes for sustained drug delivery. Biomater Adv 139:213024. https://doi.org/10.1016/j.bioadv.2022.213024
8. Santona G, Fiorentino A, Doglietto F, Serpelloni M (2024) A novel 3D printed sensorized surgical instrument to characterize pituitary adenoma: development and initial validation. In: 2024 IEEE international workshop on metrology for industry 4.0 & IoT (MetroInd4.0 & IoT). IEEE, pp 7–11
9. Bhandari S, Krishnanand SA, Taufik M (2023) 3D printing methods and materials for sensor fabrication. Mater Today Proc. https://doi.org/10.1016/j.matpr.2023.06.146
10. Khan SA, Ahmad H, Zhu G et al (2024) Three-dimensional printing of hydrogels for flexible sensors: a review. Gels 10:187. https://doi.org/10.3390/gels10030187
11. Gu J, Lee J, Kang S (2023) 3D electronic sensors for bio-interfaced electronics and soft robotics. Adv Sensor Res. https://doi.org/10.1002/adsr.202300013
12. Cafiso D, Lantean S, Pirri CF, Beccai L (2023) Soft mechanosensing via 3D printing: a review. Adv Intell Syst. https://doi.org/10.1002/aisy.202200373
13. Durgun I (2015) Sheet metal forming using FDM rapid prototype tool. Rapid Prototyp J 21:412–422. https://doi.org/10.1108/RPJ-01-2014-0003
14. Kantaros A, Soulis E, Petrescu FIT, Ganetsos T (2023) Advanced composite materials utilized in FDM/FFF 3D printing manufacturing processes: the case of filled filaments. Materials 16:6210. https://doi.org/10.3390/ma16186210
15. Li B, Zhang S, Zhang L et al (2022) Strain sensing behavior of FDM 3D printed carbon black filled TPU with periodic configurations and flexible substrates. J Manuf Process 74:283–295. https://doi.org/10.1016/j.jmapro.2021.12.020
16. Akmal J, Salmi M (2024) Additive manufacturing of self-sensing parts through material extrusion. Virtual Phys Prototyp. https://doi.org/10.1080/17452759.2024.2321200
17. Polini W, Corrado A (2023) A design for additive manufacturing tool for parts obtained through a material extrusion process. Prog Addit Manuf. https://doi.org/10.1007/s40964-023-00451-6
18. Ahammed* SR, Babu BH, Dheeraj SP, Shiferaw AY (2019) Development of sensors by 3D printing technology-fused deposition modelling. Int J Innov Technol Explor Eng 9:2182–2185. https://doi.org/10.35940/ijitee.A4757.119119
19. Ni Y, Ji R, Long K, Bu T, Chen K, Zhuang S (2017) A review of 3D-printed sensors. Appl Spectrosc Rev 52(7):623–652. https://doi.org/10.1080/05704928.2017.1287082
20. Kumar S, Singh R, Singh AP, Wei Y (2024) 3D-printed passive sensors on fabric: a state-of-the-art review and framework for future applications. Adv Mater Process Technol 11(3):1–1921. https://doi.org/10.1080/2374068X.2024.2402968
21. Jiang Y, Islam MdN, He R, Islam MN, Huang X, Cao P-F, Advincula RC, Dahotre N, Dong P, Wu HF, Choi W (2023) Recent advances in 3D printed sensors: materials, design, and manufacturing. Adv Mater Technol 8(2):2200492. https://doi.org/10.1002/admt.202200492
22. Bas J, Dutta T, Llamas Garro I et al (2024) Embedded sensors with 3D printing technology: review. Sensors 24:1955. https://doi.org/10.3390/s24061955
23. Shemelya C, Banuelos-Chacon L, Melendez A, et al (2015) Multi-functional 3D printed and embedded sensors for satellite qualification structures. In: 2015 IEEE SENSORS. IEEE, pp 1–4
24. Hassan MS, Zaman S, Dantzler JZR et al (2023) 3D printed integrated sensors: from fabrication to applications—a review. Nanomaterials 13:3148. https://doi.org/10.3390/nano13243148
25. Parmar H, Khan T, Tucci F et al (2022) Advanced robotics and additive manufacturing of composites: towards a new era in Industry 4.0. Mater Manuf Process 37:483–517
26. Saifeldeen MA, Fouad N, Huang H, Wu Z (2017) Advancement of long-gauge carbon fiber line sensors for strain measurements in structures. J Intell Mater Syst Struct 28:878–887. https://doi.org/10.1177/1045389X16665974
27. Adil S, Lazoglu I (2023) A review on additive manufacturing of carbon fiber-reinforced polymers: current methods, materials, mechanical properties, applications and challenges. J Appl Polym Sci. https://doi.org/10.1002/app.53476
28. Tang Z-H, Xue S-S, Wang D-Y, Huang P, Li Y-Q, Fu S-Y (2023) 3D printing of soft and porous composite pressure sensor with monotonic and positive resistance response. Compos Sci Technol 241:110126. https://doi.org/10.1016/j.compscitech.2023.110126
29. Dipon W, Garnsey S, Estrada M et al (2023) Development and evaluation of a fast fabrication process-based 3D printed strain gauge sensors. Ferroelectrics 611:150–160. https://doi.org/10.1080/00150193.2023.2201778
30. Gao T, Li A, Zhang X, Harris G, Liu J (2023) A data-driven process-quality-property analytical framework for conductive composites in additive manufacturing. Manuf Lett 35:626–635. https://doi.org/10.1016/j.mfglet.2023.08.050
31. Jangid AR, Strong EB, Chuang J, Martinez AW, Martinez NW (2022) Evaluation of commercially-available conductive filaments for 3D printing flexible circuits on paper. PeerJ Mater Sci 4:e21. https://doi.org/10.7717/peerj-matsci.21
32. Karimi N, Bozorgnia Tabary SAA, Fayazfar H (2024) In-depth investigation and industry plan for enhancing surface finishing of 3D printed polymer composite components: a critical review. J Appl Polym Sci. https://doi.org/10.1002/app.55494
33. Saharan LK, Agbesoyin T (2022) Design and 3D printing of a capacitive sensor for biomedical applications. In: Zonta D, Su Z, Glisic B (eds) Sensors and smart structures technologies for civil, mechanical, and aerospace systems 2022. SPIE, p 82
34. Froš D, Králová I (2023) Conductive FDM filament: electrical resistivity assessment and sensor applications. In: 2023 46th international spring seminar on electronics technology (ISSE). IEEE, pp 1–7
35. (2023) https://www.farnell.com/datasheets/3179312.pdf
36. Katsuyama H, Wu E, Koike H (2022) Using Rhythm Game to Train Rhythmic Motion in Sports. SIGGRAPH Asia 2022 Posters. ACM, New York, NY, USA, pp 1–2
37. Zanto TP, Giannakopoulou A, Gallen CL, Ostrand AE, Younger JW, Anguera-Singla R, Anguera JA, Gazzaley A (2024) Digital rhythm training improves reading fluency in children. Dev Sci 27(3):e13473. https://doi.org/10.1111/desc.13473
38. Choi Y, Kim J, Park CW, et al (2022) We play and learn rhythmically: gesture-based rhythm game for children with intellectual developmental disabilities to learn manual sign. In: CHI conference on human factors in computing systems. ACM, New York, NY, USA, pp 1–13
39. Giannaraki M, Moumoutzis N, Papatzanis Y, et al (2021) A 3D Rhythm-based serious game for collaboration improvement of children with attention deficit hyperactivity disorder (ADHD). In: 2021 IEEE global engineering education conference (EDUCON). IEEE, pp 1217–1225
40. Stano G, Di Nisio A, Lanzolla AM et al (2020) Fused filament fabrication of commercial conductive filaments: experimental study on the process parameters aimed at the minimization, repeatability, and thermal characterization of electrical resistance. Int J Adv Manuf Technol 111:2971–2986. https://doi.org/10.1007/s00170-020-06318-2

41. Protoplant Inc. 12001 NE 60th Way B2, Vancouver, Washington, 98682, United States, (2024) ProtoPasta, Conductive PLA TDS. In: https://proto-pasta.com/pages/material-data-table. https://proto-pasta.com/pages/material-data-table. Accessed 6 Feb 2025
42. Zhang J, Meng F, Ferraris E (2023) Temperature gradient at the nozzle outlet in material extrusion additive manufacturing with thermoplastic filament. Addit Manuf 73:103660. https://doi.org/10.1016/j.addma.2023.103660
43. Hoffmann K (1989) An introduction to measurements using strain gages / Karl Hoffmann
44. Ling S, Chen X, Miao L, Yin J, Jian J, Jin Q (2024) A novel semiconductor piezoresistive thin-film strain gauge with high sensitivity. IEEE Sens J 24(9):13914–13924. https://doi.org/10.1109/JSEN.2024.3373635
45. Morrison HJ;, Baer RH (1980) Microcopmputer controlled game
46. https://www.italiantechproject.it/progetti-arduino/gioco-simon Simon_game_code

Publisher's note Springer Nature remains neutral with regard to jurisdictional claims in published maps and institutional affiliations.